J. Electroanal. Chem., 171 (1984) 195–217
Elsevier Sequoia S.A., Lausanne – Printed in The Netherlands

THE METAL SIDE OF THE ELECTRICAL DOUBLE LAYER AT THE METAL/ELECTROLYTE INTERFACE

AN AB INITIO QUANTUM CHEMICAL CLUSTER STUDY

A.L.G. VAN DEN EEDEN and J.H. SLUYTERS

Van 't Hoff laboratory of Physical and Colloid Chemistry, Padualaan 8, 3584 CH Utrecht (The Netherlands)

J.H. VAN LENTHE

Theoretical Chemistry Group, State University of Utrecht, Padualaan 8, 3584 CH Utrecht (The Netherlands)

(Received 29th November 1983; in revised form 15th February 1984)

ABSTRACT

By means of quantum chemical cluster calculations the contribution of the electrode itself to the double layer capacity is established. The "metal layer" capacity C_m is defined. Model calculations have been carried out on Li clusters. The metal layer capacity is shown to be periodically distributed along the electrode surface, its value ranging from 3.6 to 5.2 μF cm^{-2}. The capacity distribution originates from coordinate-dependent charge redistribution caused by a change of electric field strength at the electrode surface. It follows that this distribution leads to a deviation from purely capacitive behaviour of a solid metal/inert electrolyte interface but does not explain the constant phase element, often found experimentally for solid electrodes.

(I) INTRODUCTION

The existence of an electrical double layer at the metal/electrolyte solution interface was ascertained by Helmholtz [1] as early as 1853. At the beginning of this century a simple theory was developed by Gouy [2] and Chapman [3] which could describe several features of double layer experiments. An essential improvement of their theory was given by Stern [4]. The Gouy–Chapman–Stern model is still reputed to be applicable in many cases. An essential feature of this theory is its one-dimensionality: the potential and charge variation are only considered in a direction normal to the electrode surface. The electrode is modelled by a conductor with a sharp boundary at which the electrode charge σ^M is homogeneously spread out.

In network analysis of the interface the electrical double layer is generally represented by a capacitor. One plate of this capacitor is formed by the metal, the other by the ions in solution, which counterbalance the charge on the electrode. This capacitor can formally be split up into two capacitors in series: one representing the

0022-0728/84/$03.00

inner layer and one representing the diffuse double layer [5]. By experiment one can only obtain the total capacity. The contribution of the diffuse double layer to the total capacity can be calculated by the Gouy–Chapman–Stern theory. This leaves the inner layer capacity as the unknown quantity. Several models have been proposed for the inner layer, which, in the absence of specific adsorption, are based on the solvent dipole orientation of the first solvent layer(s) adjacent to the electrode surface [6]. In these models the electrode is still regarded as a homogeneous reservoir of electrons with a sharp boundary, although the solution now has a three-dimensional structure. That also the electrode itself is important in double layer theory was considered as early as 1928 by Rice [7]. Recent model calculations include the influence of the metal [8]. Kornyshev et al. [9] used a non-local electrostatic approach to the interface and showed that a model with a diffuse boundary gave better results than one with a sharp boundary. Recently, Badiali et al. [10] calculated the contribution of the metal to the inner layer capacity. Their model for the electrode was a one-dimensional one with an a priori fixed shape of the electron-density profile. They showed [11] that neglecting the solvent structure did not change their results.

For the metal/vacuum interface, Smoluchowski [12] showed in 1941 that the metal structure had a predominant effect on the electronic work function. He could explain successfully the differences in electronic work function found experimentally for single crystals by taking into account the three-dimensional surface charge-density profile of those crystals.

In this paper we study the influence of the atomic structure of the electrode on the metal/solution interfacial behaviour. It has already been known for a long time that solid metal electrodes display a deviation from purely capacitive behaviour. The interfacial impedance is generally described by the so-called constant phase element. A physical model of it is lacking. From experiments we can deduce that the atomic structure of the electrode may be responsible for the observed interfacial behaviour, i.e. the three-dimensional surface charge-density profile of the metal contributes to the properties of the inner layer capacity.

We have performed calculations on model electrodes with a definite crystalline structure. The macroscopic metal/solution interface was modelled by clusters with a single crystal atomic arrangement. An electric field was then applied to the cluster. In this way a three-dimensional charge-density profile was obtained as a function of potential, leading to a distribution of capacities on the electrode surface. This distribution was compared with the one generally used for the interpretation of the experimental results.

(II) EXPERIMENTAL

In this section we present an impedance study of a gold single crystal/inert solution interface (Section II.1). The interfacial behaviour of the gold electrode is compared with the ideal interfacial behaviour of a dropping mercury electrode (DME) and the so-called constant phase element is described, which in general

represents the frequency dependence of the interface between a solid metal electrode and an electrolyte solution. In Section (II.2) a phenomenological explanation is proposed for the observed solid metal/solution interface characteristics.

(II.1) The interfacial impedance of gold single crystal electrodes

By means of the ac-impedance technique we studied the electrical double layer at single crystal gold electrodes in 1 *M* perchloric acid. The impedance analysis was performed as described by Sluyters et al. and measured with the experimental set-up described in ref 13. The frequency characteristic of the electrical interface is shown in Fig. 1 in which the impedance is plotted in a complex-plane representation [14].

The dashed line in Fig. 1 shows the frequency characteristic of a DME in an inert electrolyte solution at a potential in the ideally polarisable region. The impedance is represented by a straight line perpendicular to the abscissa, showing ideal interfacial behaviour. In terms of an equivalent circuit, the interfacial behaviour of the DME at

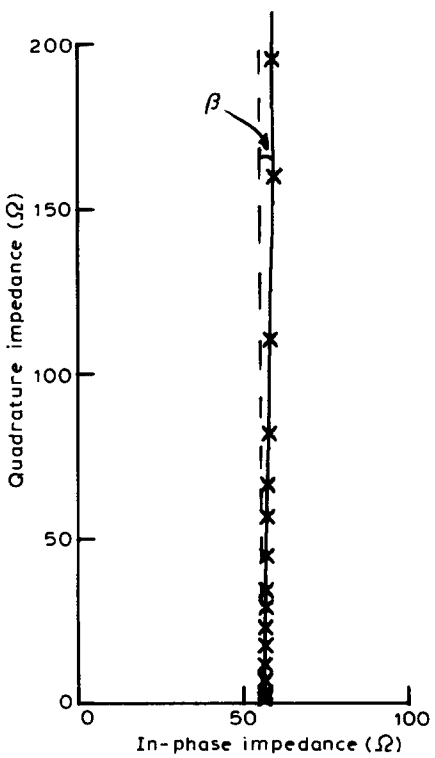

Fig. 1. Complex plane representation of the impedance of an Au (100) single crystal in 1 *M* $HClO_4$. Potential within the ideally polarisable region (———). Frequency range between 80 and 20,000 Hz. (— — —) *RC*-type behaviour.

one potential is represented by one capacitor (Fig. 2a). It is evident from Fig. 1 that there is a difference between the DME and the Au (100) solid electrode. By rotating the line for the DME clockwise through an angle of β radians one gets the frequency characteristic of the gold electrode and a one-to-one mapping of the frequency points can be constructed. This constant phase shift, with respect to the DME, ranges from 0.5 to 1.5°, depending on the gold single crystal face and potential. This constant phase shift is a generally observed phenomenon for solid electrodes. At solid/solid interfaces constant phase shifts are also observed that range from 1 to 2° [15]. The interfacial behaviour of a solid electrode is represented by the so-called "constant phase element" (CPE), which can be constructed of passive circuit elements as shown in Fig. 2b: instead of one capacitance there are many combinations of a capacitance (C_i) and a resistance (R_i) in series, all R_iC_i combinations parallel to each other, giving rise to a distribution in RC times.

The interfacial impedance Z of a solid electrode can be expressed mathematically as

$$Z = R(j\omega RC)^{\alpha-1} \tag{1}$$

with $j = \sqrt{-1}$ and ω = angular frequency. α is a rotation parameter. Its value ranges between 0 and 1. $\alpha\pi/2$ represents the angle β. Equation (1) implies a distribution function of RC times. R_0C_0 is the mean value of the distributed RC times, if expressed on a logarithmic RC scale. The distribution function $F(s)$ is, with

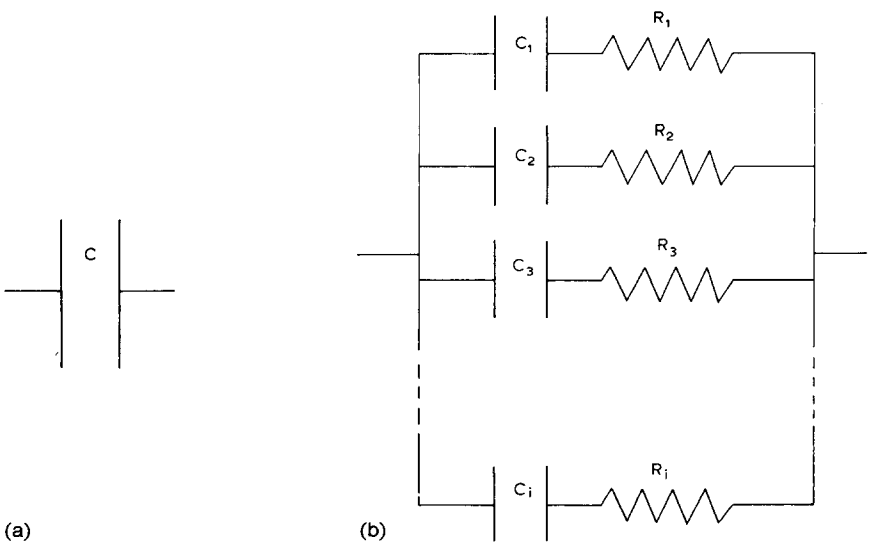

Fig. 2. Equivalent circuit representation of the electrical interface in the ideally polarisable region; (a) for a DME, (b) for a solid electrode.

$$s = \ln(RC/R_0C_0),$$

$$F(s) = \frac{1}{2\pi} \frac{\sin \alpha\pi}{\cosh(1-\alpha)s - \cos \alpha\pi} \tag{2}$$

This expression is analogous to the one given by Cole and Cole [16] for dielectric relaxation and can be derived following the general procedure outlined in ref. 17. The rotation parameter α determines the width of the distribution, see Fig. 3.

(II.2) Phenomenological explanation

What can be the reason for a distribution of RC times representing the electrical interface at a solid electrode? By working under very precise conditions with very clean materials the influence of contamination was minimised. Frequency dispersion due to uneven current density distribution was avoided by careful cell construction. Moreover, the electrodes were monocrystalline and smoothly polished. As the measurements are reproducible the only difference between a DME and a solid electrode is the crystalline nature of the latter. On an atomic scale the electrode surface can be considered as "rough". This leads to a charge distribution on the electrode surface, which will be periodical, depending on the crystal face which

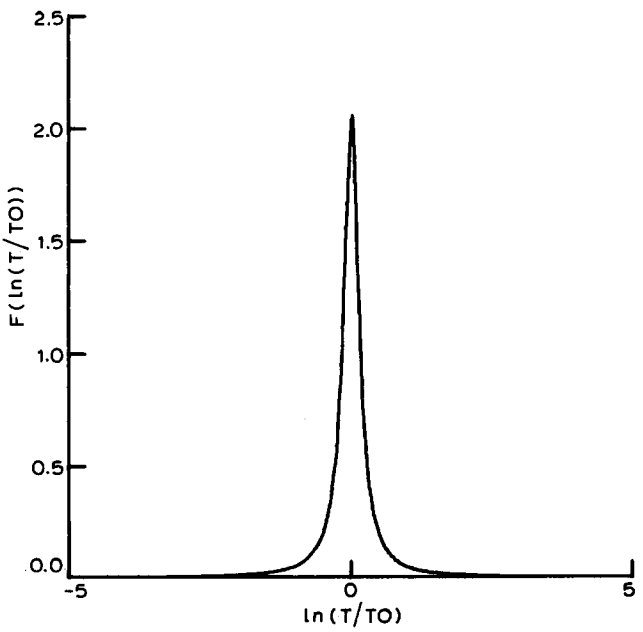

Fig. 3. Cole and Cole distribution function with $\alpha = 0.05$ rad.

forms the electrode surface [12]. This charge distribution might be the cause of the observed CPE. In order to check this, it is necessary to get detailed information on the electrode/solution interface at an atomic level. Quantum mechanics, and more specifically quantum chemical methods, are well suited for this purpose, enabling one to obtain the charge distribution as a function of coordinates and as a function of potential, which is necessary for calculating capacities. In this way we get the contribution of the metal to the differential double layer capacity and can find out if the distribution in capacities explains the CPE behaviour.

(III) QUANTUM CHEMICAL CLUSTER CALCULATIONS

In this section the calculational procedure for obtaining capacities on an atomic scale is demonstrated on the so-called ion lattice model (Section III.1). The application of this procedure to real clusters is outlined in Section (III.2). The calculation set-up is then described in Section (III.3). By studying Li clusters of varying number of atoms the necessary size of the cluster is established (Section III.4). Results are given in terms of a distribution of capacities and are related to experiments (Section IV).

(III.1) Definition of the metal layer capacity

In the ion lattice model [18] a metal is considered as consisting of positive nuclei on fixed grid points and of a homogeneous distribution of negative charge (electrons) throughout the metal as depicted in Fig. 4a. The bulk of the metal can be thought of as being made up of electroneutral units, the so called Wigner–Seitz cells [19], which contain one nucleus, centred in the middle of the cell. The boundary of such a cell lies at half a grid length (d) from the center.

By cleaving the metal one obtains two halves which can be considered as electrodes. The condition of electroneutrality implies that the cleaving must take place at the boundary, z_b, between two Wigner–Seitz cells (Fig. 4a), which becomes the location of the metal–vacuum interface. The discontinuity in the homogeneous charge distribution at the interface is energetically unfavourable and a relaxation of the charge distribution across the interface will take place. There will be a "spill over" of charge as is modelled in Fig. 4b. The nuclei are kept fixed in their locations. The total charge $-Q$ outside the metal (with boundary z_b) leaves a charge deficiency $+Q$ inside the metal compared with the unrelaxed situation.

By applying an external electric field E perpendicular to the electrode surface, there will be a redistribution of charge, e.g. an extra amount of charge $-\Delta Q$ will come on the outside of the metal, leaving an extra deficiency of ΔQ on the inside (Fig. 4c). The induced charge redistribution is the difference in charge distribution with an external electric field and without it and is depicted in Fig. 4d. This spatial charge separation forms a capacity, the metal layer capacity C_m. The distance between the centres of both induced charge distributions, z_m^+ and z_m^-, respectively,

determines the value of this capacity, where

$$z_m^+ = \frac{\int_{-\infty}^{z_b} \Delta Q(z)(z_b - z)\mathrm{d}z}{\int_{-\infty}^{z_b} \Delta Q(z)\mathrm{d}z} \tag{3a}$$

$$z_m^- = \frac{\int_{z_b}^{\infty} \Delta Q(z)(z - z_b)\mathrm{d}z}{\int_{z_b}^{\infty} \Delta Q(z)\mathrm{d}z} \tag{3b}$$

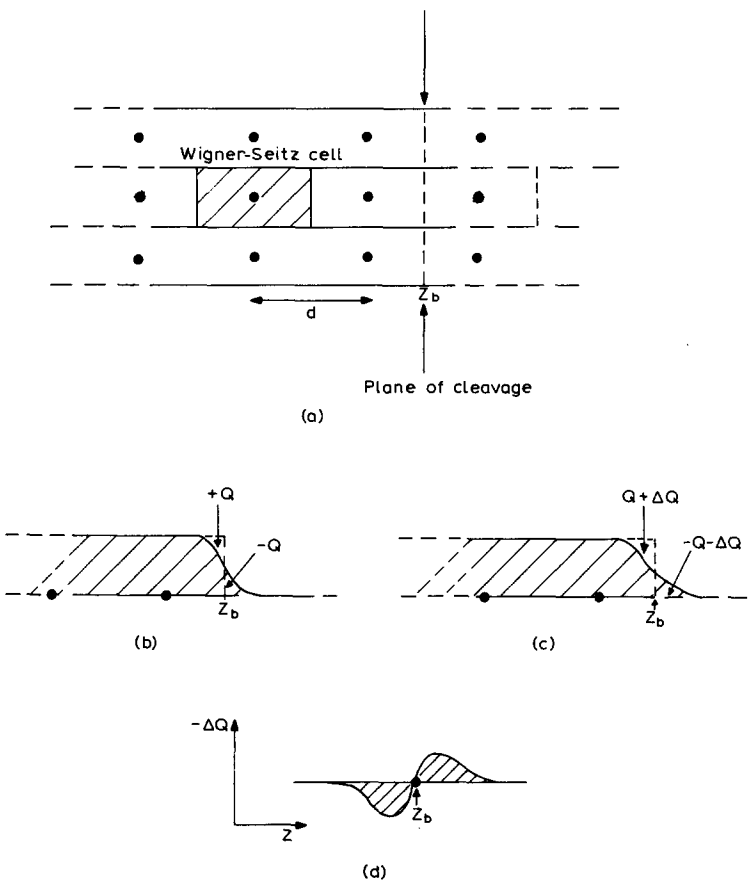

Fig. 4. Two-dimensional schematic representation of the construction of an electrode and calculation of the metal layer capacity C_m. (a) Ion lattice model of a metal with Wigner–Seitz cells. Cleaving of metal on cell boundary z_b. d = grid length. (b) Relaxation of electronic charge to $z > z_b$. (c) Charge profile around interface with external field E. (d) Induced charge density difference profile, obtained by subtraction of the values in (b) from those in (c).

The value of the metal layer capacity is then

$$C_m = 1/4\pi(z_m^+ + z_m^-) \tag{4}$$

We shall show that the definition (4) of C_m can also be obtained starting from the one-dimensional Poisson equation for the charge redistribution. The Poisson equation is

$$\nabla^2 V(z) = -4\pi\rho(z) \tag{5}$$

which can be rewritten as

$$V(z) = -4\pi\int_{-\infty}^{z} \rho(z')\cdot(z - z')\mathrm{d}z' \tag{6}$$

Whence

$$V^+(z_b) = -4\pi\int_{-\infty}^{z_b} \rho(z')\cdot(z_b - z')\mathrm{d}z' \tag{7a}$$

and

$$V^-(z_b) = -4\pi\int_{z_b}^{\infty} \rho(z')\cdot(z' - z_b)\mathrm{d}z' \tag{7b}$$

With

$$\int_{-\infty}^{\infty} \rho(z)\mathrm{d}z = 0 = \int_{-\infty}^{z_b} \rho(z)\mathrm{d}z + \int_{z_b}^{\infty} \rho(z)\mathrm{d}z = +\Delta Q - \Delta Q = 0 \tag{8}$$

and eqn. (4) one obtains:

$$C_m = \frac{1}{4\pi}\cdot\left[\frac{1}{4\pi}\left(\frac{V^-}{\Delta Q} - \frac{V^+}{\Delta Q}\right)\right]^{-1} = \frac{\Delta Q}{V^- - V^+} = \frac{\Delta Q}{\Delta V} \tag{9}$$

If the induced charge distribution across the metal boundary is known, eqn. (3a and b) can easily be applied and eqn. (4) will give the interfacial metal layer capacity C_m.

(III.2) Calculation of the metal layer capacity at real clusters

In the actual calculation we are interested in the influence of the crystallographic structure of the electrode. An ion lattice model of the electrode does not satisfy this requirement as its charge variation is only defined in one direction. Ab initio Hartree–Fock cluster calculations lead to the required coordinate- and potential-dependent charge (re)distributions.

A cluster has a finite size. A straightforward application of formulas (3) and (4) is therefore not possible in this case: the indefinite integration limits must be adjusted. In the calculations, we have taken the middle of a cluster as the origin and the place where the charge density becomes negligible as the upper limit of the integration. We further established that, by taking $z_m^+ = z_m^-$ in eqn. (4), thus avoiding the calculation of z_m^+, the result of the calculation differed from the more precise and expensive one by less than 9%. So, as a reliable estimate of C_m we have taken

$$C_m = 1/4\pi(z_m^- + z_m^-) \tag{10}$$

The capacity as a function of coordinates was calculated by imagining the crystal to be cut in equally sized columns perpendicular to the crystal face under consideration as shown in Fig. 5, thereby dividing the cluster into many smaller parts. For each column the capacity was calculated as described above.

(III.3) Calculation set-up

As we are interested in the induced charge redistribution on the metal side of the double layer with a change of potential, we restrict our calculations to the metal, omitting the contribution of the solution to the double layer capacity. The potential drop (V) across the interface is represented by an external electric field (E) perpendicular to the electrode surface. From double layer theory it is known that the field strength in the inner layer is of the order of 10^5 to 10^8 V cm^{-1}. It is reasonable to use these values for our calculations. As our main interest lies in a qualitative description and understanding of the influence of the metal on double layer characteristics, we take lithium as a representative of more practical metals like e.g. copper and gold. This is reasonable because lithium is also an *sp* metal and, moreover, with lithium there is the advantage that calculations can be carried out on clusters of a relatively large size (20–24 atoms) within the framework of an ab initio self-consistent-field procedure. For solving the time-independent Schrödinger equation

$$H\psi(r) = \epsilon\psi(r) \tag{11}$$

with H the Hamiltonian, $\psi(r)$ the electronic wavefunction and ϵ the eigenvalue of this operator equation, one has to use approximations. Within the Born–Oppenheimer restriction the Hamiltonian H is

$$H = -\tfrac{1}{2}\sum_i \nabla_i^2 + \sum\sum_{\alpha<\beta} \frac{Z_\alpha Z_\beta}{r_{\alpha\beta}} + \sum\sum_{i<j} \frac{1}{r_{ij}} - \sum\sum_{i\ \alpha} \frac{Z_\alpha}{r_{i\alpha}} \tag{12}$$

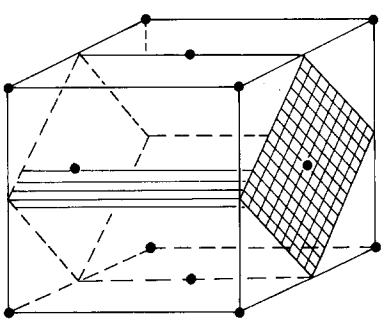

Fig. 5. Schematic representation of the division of the cluster around the central surface atom in many small columns.

The electronic wavefunction $\psi(r)$ is approximated by a single Slater determinant in the Hartree–Fock method and is found by solving eqn. (11) by an iterative procedure until self-consistency is reached. This is done by the Roothaan method [20].

For lithium we used a minimal basis set of Gaussian-type orbitals including a set of $2p$ Gaussians, using the exponents and contraction coefficients of Van Duijneveldt [21] (see Table 1). The $2p$ exponent was optimised for the ^2P excited state of lithium [22].

The external electric field E can be introduced as a perturbation to the Hamiltonian H of eqn. (12), which gives as the Hamiltonian H' [23]

$$H' = H + \sum_{\mu} E \cdot z_{\mu} \tag{13}$$

where z_{μ} is the coordinate of the μth electron in the external field E. Throughout this paper the value of E was taken as 0.01 atomic units (a.u.), which is approximately 5×10^7 V cm^{-1}. The chosen field strength is rather high, but is within the limits of accurate perturbation calculations.

The calculations were performed with a CYBER 175 computer using local versions of IBMOLH-integral, SCF and property programs [24]. For instance, a calculation on a cluster of 22 Li atoms involves the evaluation of 14,540,495 integrals and takes about 14 h computer time.

(III.4) Choice of cluster size

A crucial point in cluster calculations is the size of the cluster in relation to the parameters that are of interest. It is a well-known fact that bulk properties converge only slowly with increasing cluster size [25]. As we are interested in the correct charge distribution around the interface (see eqns. 3 and 4), which might converge slowly with cluster size as well, we have focussed our attention on that problem.

(III.4.a) Linear clusters

The influence of bulk depth on the charge distribution was tested by means of

TABLE 1

Lithium basis set

	Exponent	Coefficient
$1s$	101.390	0.020829
	15.3116	0.138816
	3.40235	0.447529
	0.87357	0.528307
$2s$	0.08000	0.403662
	0.03300	0.665602
$2p$	0.047	1.0

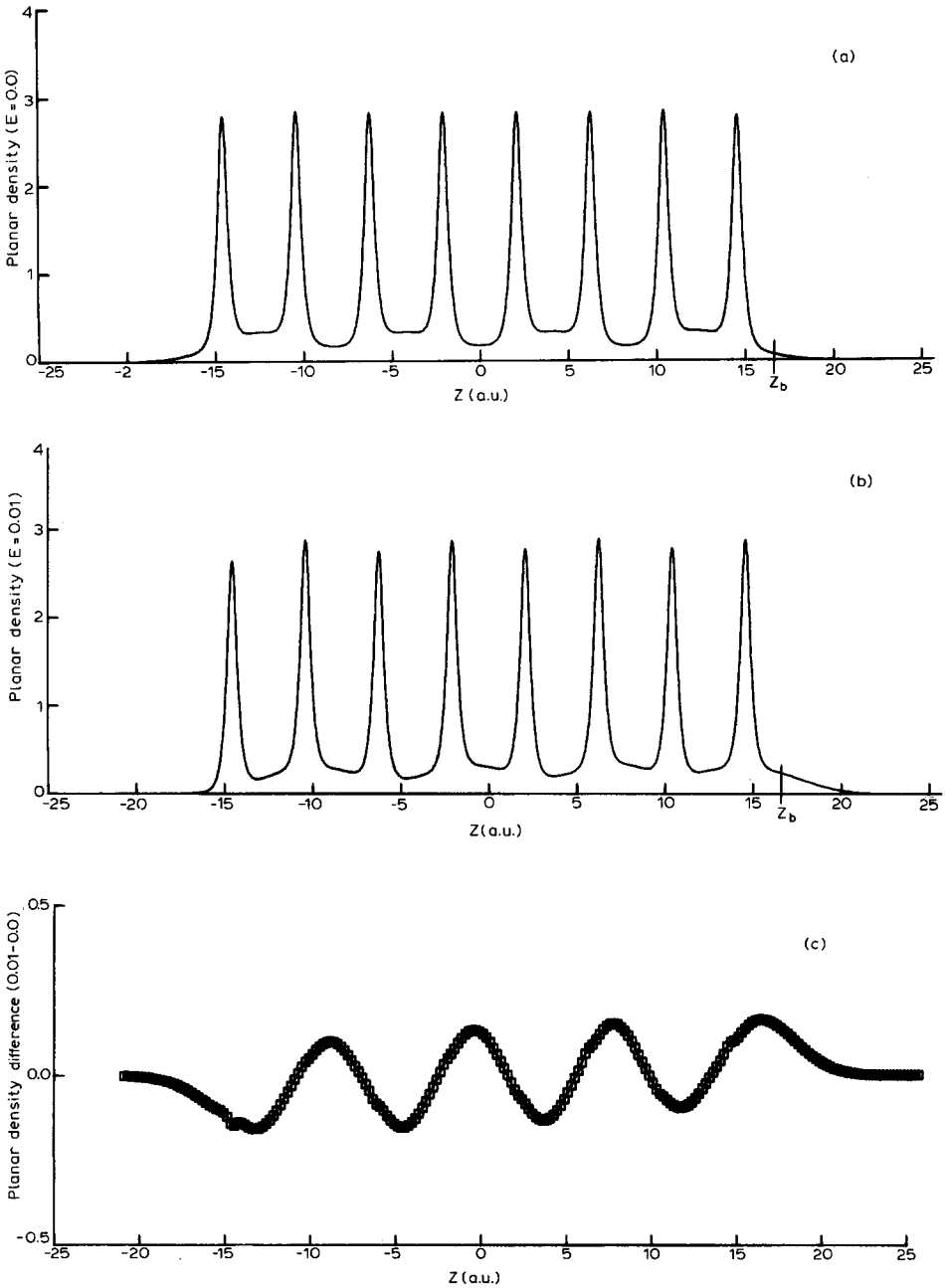

Fig. 6. Li(8)line; charge profiles. (a) Planar charge density along z-axis without electric field E; z_b = physical boundary of the cluster lying along the z-axis. (b) Same as (a), but with $E = 0.01$ a.u. (c) Induced planar density difference, obtained by subtracting the values in (a) from those in (b).

linear clusters of varying length, ranging from two to twelve Li atoms in a row. The interatomic distance was taken from the literature [26]: for a face-centered cubic packing the plane-to-plane distance for a (100) plane is 4.1612 a.u. In order to be able to make comparisons with (100) clusters we have taken this interplanar distance as the interatomic distance in the linear clusters. A typical result is depicted in Fig. 6 for a Li cluster of 8 atoms in a row. In Fig. 6a and b the planar charge density $\rho_{xy}(z) = \int_x \int_y \rho(x, y, z, E)\mathrm{d}x\mathrm{d}y$ without and with electric field is plotted as a function of the z-coordinate. The linear cluster lies along the z-axis.

The planar charge density extends beyond the physical boundary of the cluster. With the electric field E along the z-axis, charge is "pushed inwards" on the left-hand side and "pulled outwards" on the right-hand side of the Li cluster, giving two results in one calculation, namely the induced charge distribution at $E = -0.01$ a.u. and at $E = 0.01$ a.u. The induced planar charge redistribution (Fig. 6c) shows an oscillatory behaviour. The period of the oscillation is twice the interatomic distance. This may be understood by only considering the mixing of the Lowest Unoccupied Molecular Orbital (LUMO) into the Highest Occupied MO (HOMO) when the cluster is polarised. Hückel theory [27] already explains a periodicity of twice the Li–Li interatomic distance in the charge shift.

Figure 7 shows the potential difference for the Li(8) line with field E and without it. It is clear that the external field is compensated inside the cluster, as is to be expected for a conductor. At a great distance from the cluster the potential is determined by the external field as $V = E \cdot z$.

The calculated values of the metal capacity are presented in Table 2. With an increasing number of Li atoms the capacity decreases in a way that suggests slow convergence. However, the decrease is small: going from two to twelve atoms in a row changes the capacity by about 10%. We conclude that with a depth of 3 or 4 atoms the cluster calculations will give a reasonable estimate of the capacity.

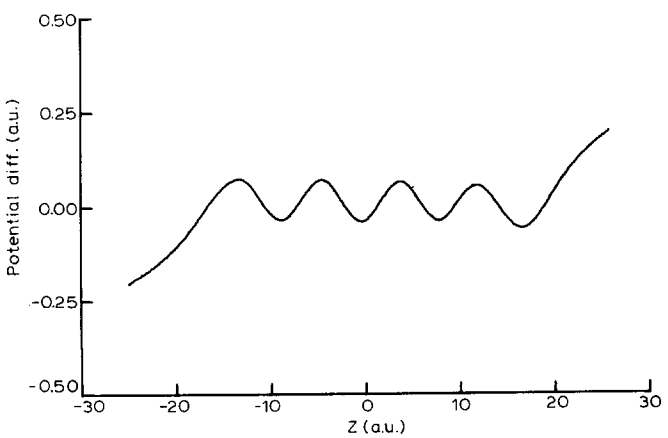

Fig. 7. Li(8) line: potential difference profile ΔV along z-axis. At a great distance from the cluster boundaries ΔV follows the undisturbed field.

TABLE 2

Metal layer capacity C_m for linear clusters vs. chain length

Number of lithium atoms	Capacity/μF cm^{-2}
2	5.67
4	5.44
6	5.32
8	5.20
10	5.07
12	4.95

changes the capacity by about 10%. We conclude that with a depth of 3 or 4 atoms the cluster calculations will give a reasonable estimate of the capacity.

(III.4.b) Three-dimensional clusters

The influence of the bulk width can be established in a way which is analogous to that described in Section (III.4.a). For a (100) single crystal all surface atoms have identical surroundings. We can therefore restrict ourselves to an adequate description of the charge distribution around one surface atom, for which there is little

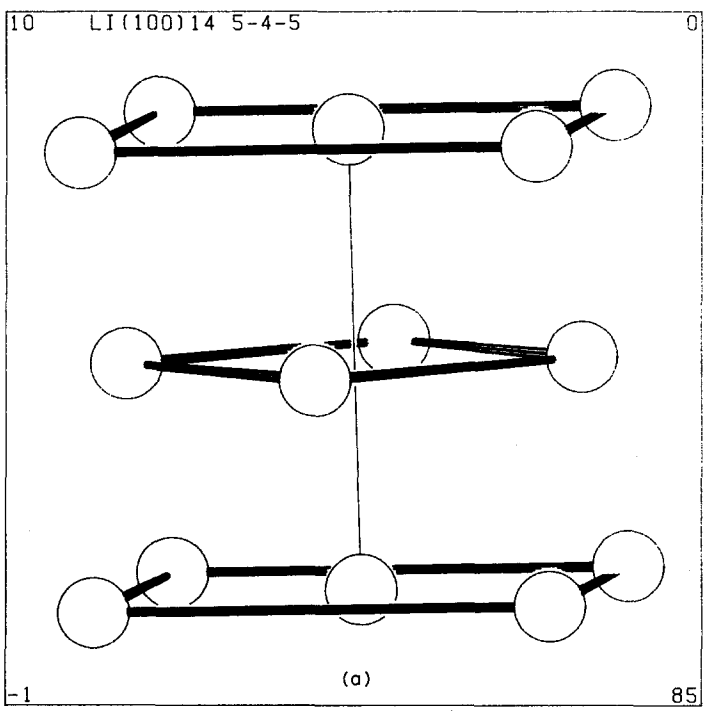

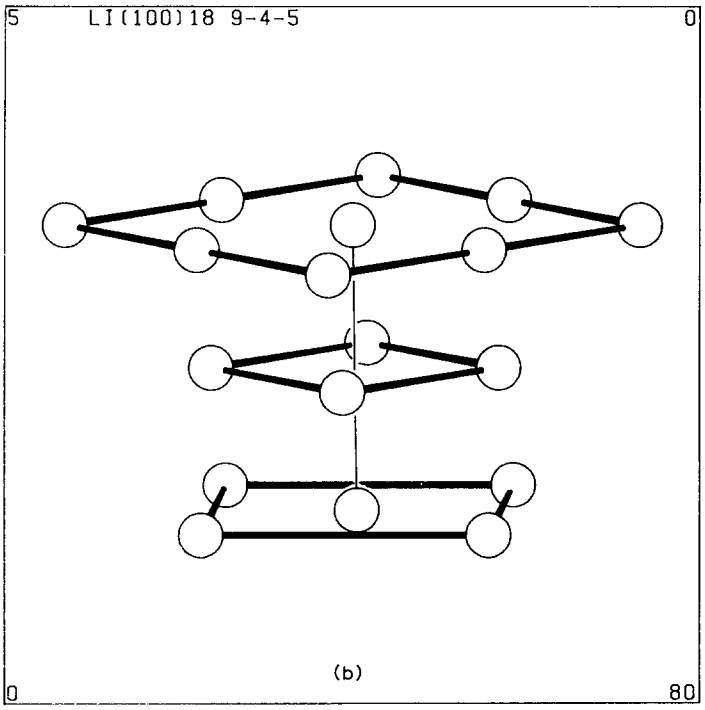

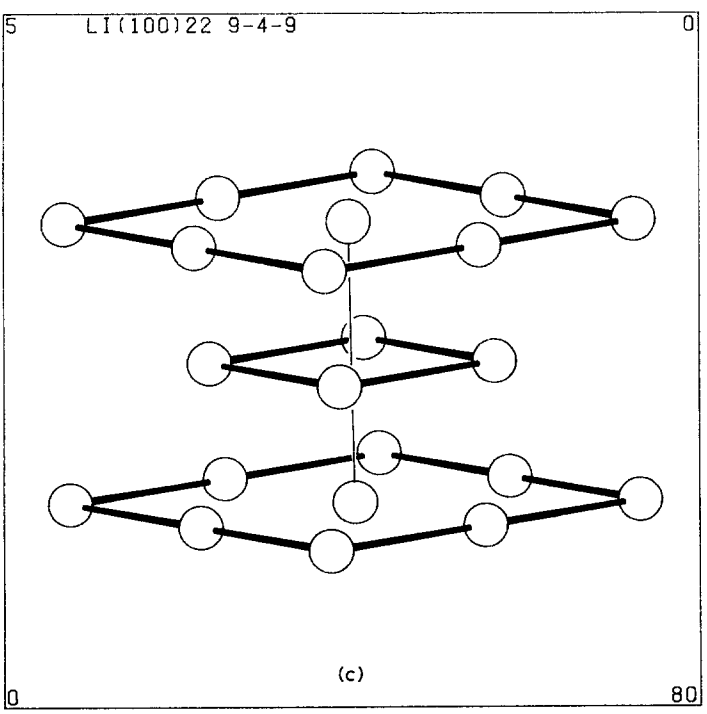

Fig. 8. Models of the Li clusters used in this work. (a) Li (100) 5-4-5; (b) Li (100) 9-4-5; (c) Li (100) 9-4-9.

disturbance from the edges of the cluster. This also applies to other single crystal faces. So, if extension of the cluster by more atoms in whatever direction does not lead to an appreciable change in the charge distribution around the central atom, then the cluster will do for our purpose.

We chose three clusters. As a first cluster we took the primitive f.c.c. cell, whose boundary planes are (100) planes. The central atom of such a (100) plane has all its nearest neighbours in the first, second and third layers and four second-nearest neighbours in the third layer (see Fig. 8a). In a shorthand notation we will denote

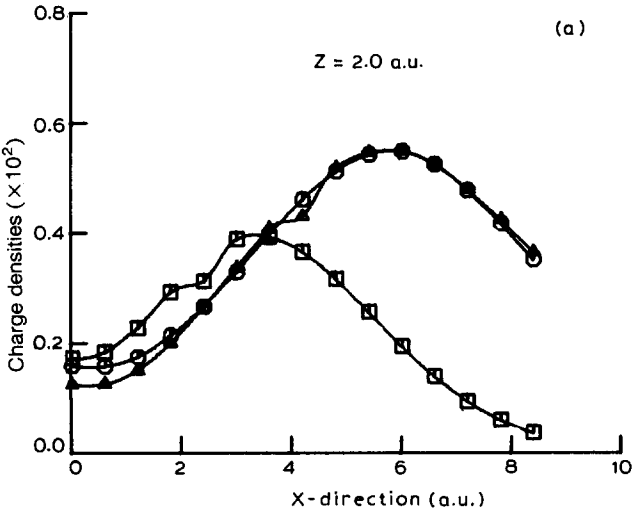

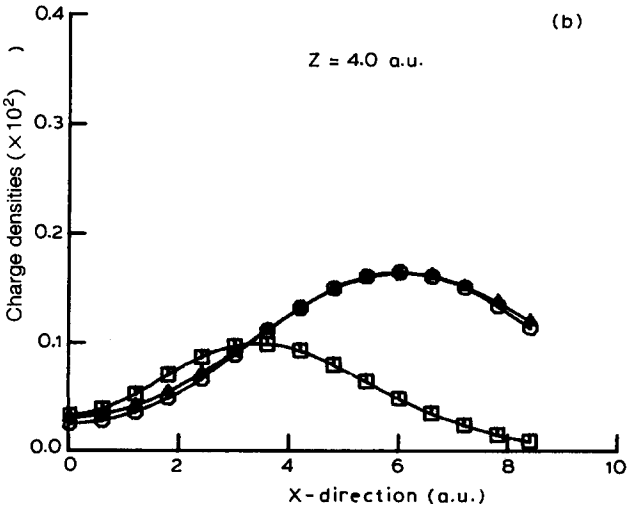

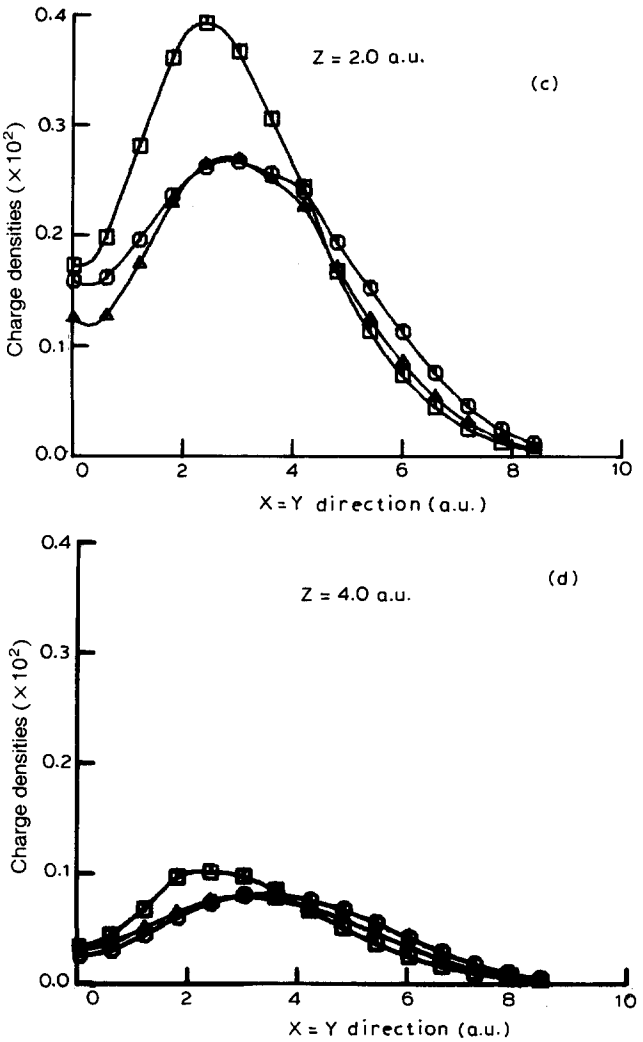

Fig. 9. Charge density profile for three Li clusters along the (100) plane in two characteristic directions at two altitudes without electric field. (□) Li (100) 5-4-5; (○) Li (100) 9-4-5; (△) Li (100) 9-4-9.

this as a Li (100) 5-4-5 plane, i.e. five atoms in the first (= surface) layer, four in the second and five in the third layer. The second cluster is the same as the first, but extended with four atoms in the first layer: Li (100) 9-4-5 (see Fig. 8b). The third one also has four extra atoms in the third layer and can be denoted by Li (100) 9-4-9 (Fig. 8c).

For these three clusters we calculated point charge densities around the central atom without and with external electric field and compared the results. Figure 9

gives charge densities in two typical directions starting from the central atom that is situated at $(x, y) = (0, 0)$, without field and at two different heights above the plane $(x, y, z = 0)$, in which the nuclei of the surface atoms lie. The physical boundary of the cluster-electrode lies at $z = 2.0806$ a.u., so $z = 2.0$ a.u. is within and $z = 4.0$ a.u. is well outside the electrode surface. It is evident from Fig. 9 that the Li (100) 5-4-5 cluster gives a charge-density profile that is quite different from those of the other two clusters. The latter two give approximately the same result. Evidently it is

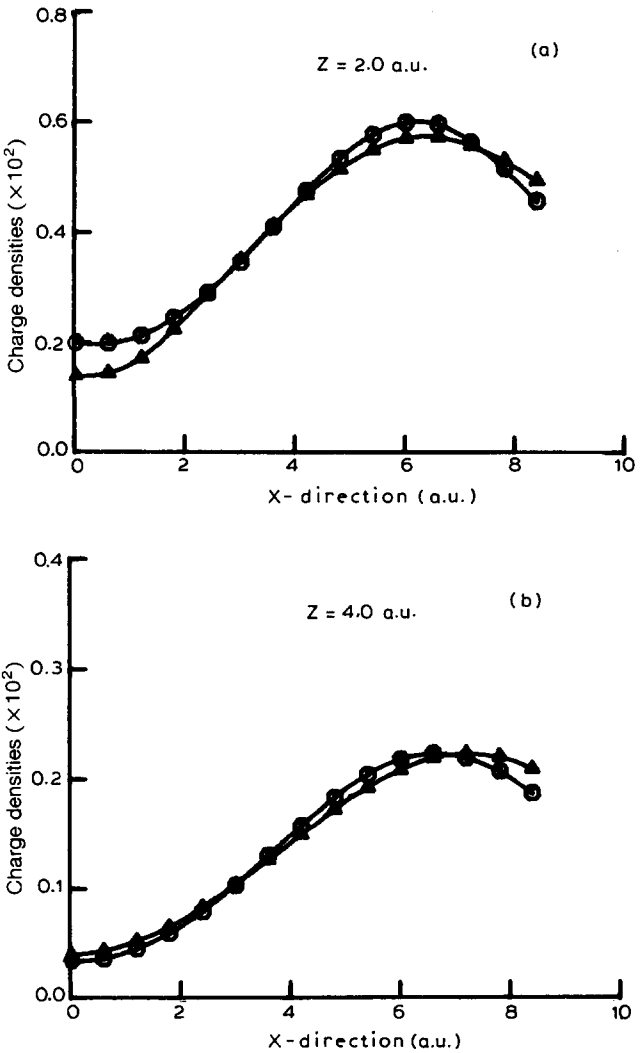

Fig. 10. As Fig. 9, for the two biggest clusters in the presence of an electric field of 0.01 a.u. (○) Li (100) 9-4-5; (△) Li (10) 9-4-9.

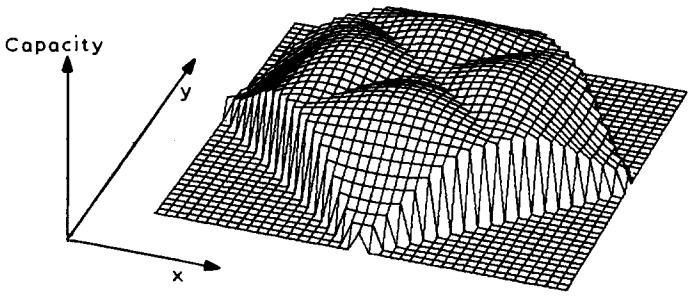

Fig. 11. Capacity profile around the central surface atom. the base is the same as in Fig. 5.

necessary to have at least nine atoms in the first layer in order that the central atom is sufficiently well surrounded.

We therefore rejected the Li (100) 5-4-5 cluster and calculated the charge densities for Li (100) 9-4-5 and Li (100) 9-4-9 with an applied external electric field of 0.01 a.u.. The results are shown in Fig. 10. Again there are no essential differences between the two clusters. For the calculation of capacities we chose the Li (100) 9-4-9 cluster for two reasons. The first reason is that, although calculations on the Li (100) 9-4-5 cluster are cheaper and faster, its lack of D4h symmetry introduces a permanent dipole along the main axis. This could cause some distortion of the results, which is not visible in the previously mentioned comparisons, but can interfere at lower field strengths. The second reason is that the symmetrical 9-4-9 cluster actually has two surfaces, both perpendicular to the electric field. The field direction is opposite for either surface, allowing one to get two results from one SCF calculation.

(IV) RESULTS

The capacity distribution on the electrode surface

In Fig. 11 the calculated capacity profile for the Li (100) 9-4-9 cluster is shown. The cluster was divided into columns with a base of 0.20806 by 0.20806 a.u. By sampling the capacity values a histogram can be made of the frequency with which a capacity value occurs vs. the value itself. See Fig. 12.

(V) DISCUSSION

It is evident from Fig. 12 that the capacity is distributed over the surface. Its value ranges from 3.6 to 5.2 μF cm^{-2}. There is a sharp peak at 4.85 μF cm^{-2} and a long tail to lower capacity values. In Section (III.4.a) we found capacities in the same range for linear clusters, so from them already a reliable estimate of the value of the capacity can be obtained.

The calculated capacities are one order of magnitude smaller than those found

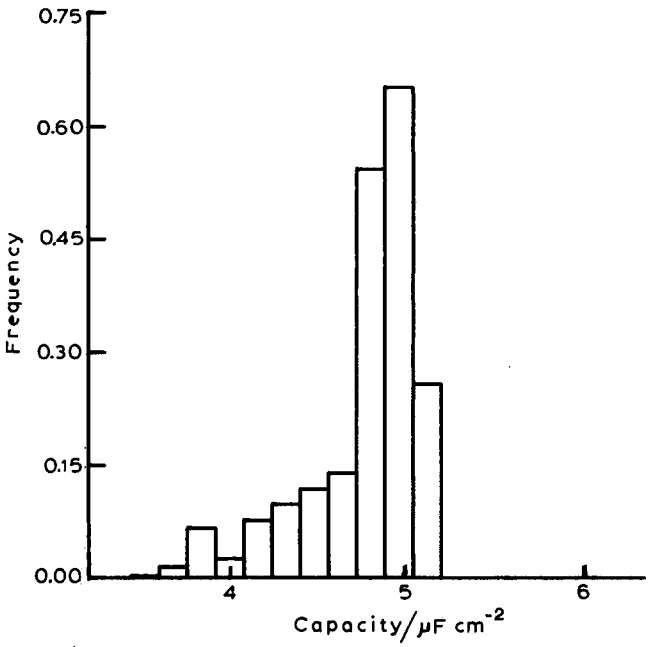

Fig. 12. Histogram of the capacity values of a Li (100) plane.

experimentally. For instance, on gold single crystals the capacity values range from 25 to 40 μF cm^{-2} in 1 M $HClO_4$, depending on electrode potential. In view of the realistic description of the electrical double layer being composed of three condensers in series as stated by Badiali et al. [10], i.e. the metal layer capacity C_m, the diffuse layer capacity and the solution-side inner layer capacity, it must be concluded that the value of C_m in the presence of an electrolyte phase has a value appreciably larger than its value in vacuum. A plausible explanation will be a restriction of the spill-over of electrons by the adjoining electrolyte solution.

It should be kept in mind that we applied a rather high external electric field to the cluster. Our calculations, therefore, do not lead to a differential double layer capacity *per se*, but to a realistic approximation of the differential double layer capacity.

By analogy with the Cole and Cole distribution, which is best described on a logarithmic scale, we transposed the histogram to a logarithmic scale and fitted a distribution function by means of a polynomial. This is shown in Fig. 13a. Figure 13b shows the frequency characteristic of the impedance that corresponds to this distribution and that is calculated by the expressions for the admittance:

$$Y'(\omega) = \int \frac{\omega^2 R C^2 F(s)\,ds}{1 + \omega^2 R^2 C^2} \tag{14}$$

$$Y''(\omega) = \int \frac{\omega C F(s)\,ds}{1 + \omega^2 R^2 C^2} \tag{15}$$

with $s = \ln(C/C_0)$, which gives the in-phase and quadrature impedance as

$$Z' = Y'/(Y'^2 + Y''^2) \tag{16}$$

$$Z'' = Y''/(Y'^2 + Y''^2) \tag{17}$$

For R we took the experimentally reasonable value of 8 Ω cm^2. The integration limits were $s = -0.34$ and $s = 0.08$ respectively. It follows that the asymmetric distribution function does not produce a *constant* phase element: i.e. the phase angle β changes in the frequency range considered. Note that the abscissa in Fig. 13b is magnified 60-fold to show the effect more clearly.

If we look more carefully at Fig. 12 a slight shoulder or hump can be seen on the low capacity side. We think that this phenomenon is caused by the atoms in the second layer, that lack some of their nearest neighbours. This may cause incorrect estimation of the contribution of the second layer to the surface-charge profile. Addition of more atoms to the second layer was not possible because of limited computer facilities (8 atoms would have to be added then).

Yet, even if we neglect the slight shoulder, the calculated distribution function still remains asymmetric. If, in spite of the evident asymmetry, a symmetrical Cole and Cole distribution function is fitted to our histogram (Fig. 14), the concomittant phase angle β is found to amount to 1.1°, which is a value remarkably close to our experimental value obtained for a perfect (100) gold crystal face.

It should be realised that our results have been calculated for a metal/vacuum interphase. The calculated capacity of the metal side of the inner layer need not

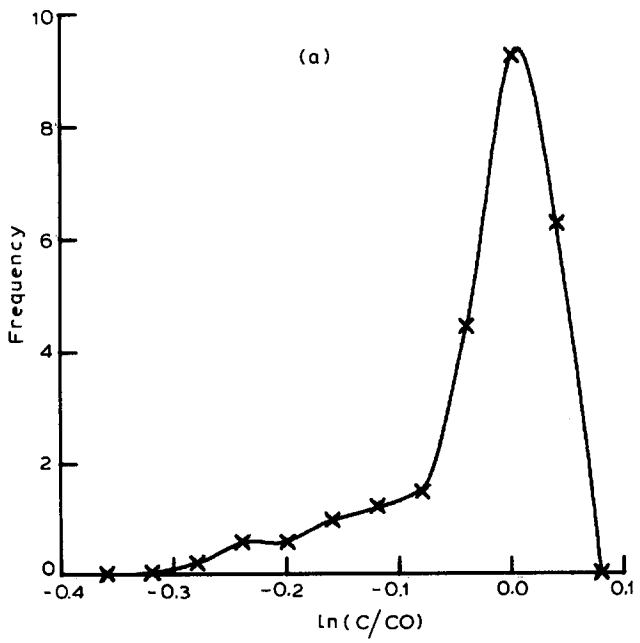

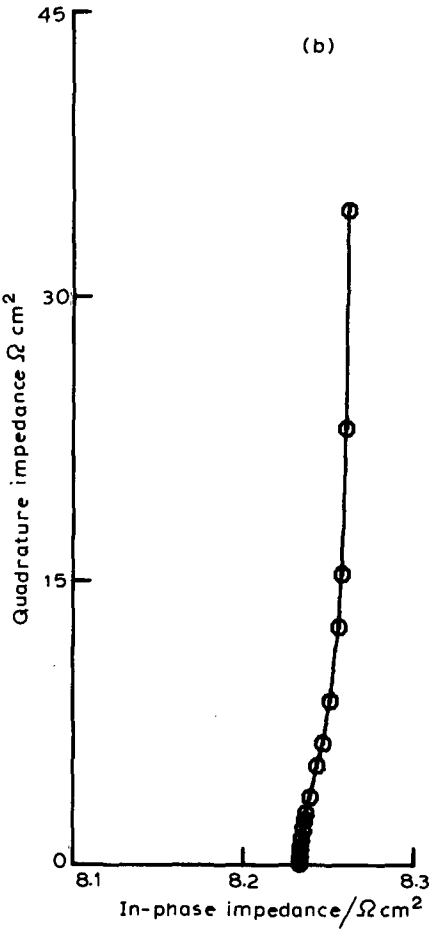

Fig. 13. Calculated distribution function for the capacity profile of a Li (100) plane. (a) Polynomial fit to the histogram of Fig. 12 on a logarithmic scale. (b) Complex plane representation of resulting impedance. Frequency range between 80 and 20,000 Hz.

necessarily be identical to the one for the metal/electrolyte interphase. For in the presence of an electrolyte solution containing discrete charges, the electric field, that in our calculations has been supposed to be homogeneous, will be inhomogeneous. Moreover, the presence of oriented water molecules will contribute to the local field strength. This makes it difficult, as yet, to connect a change of field strength to a more practical potential scale. We plan to study this.

The way in which this electrochemical problem has been treated quantum mechanically offers the possibility to make a comparative study of electrodes with different single crystal faces as a function of potential. This will be the subject of a forthcoming paper.

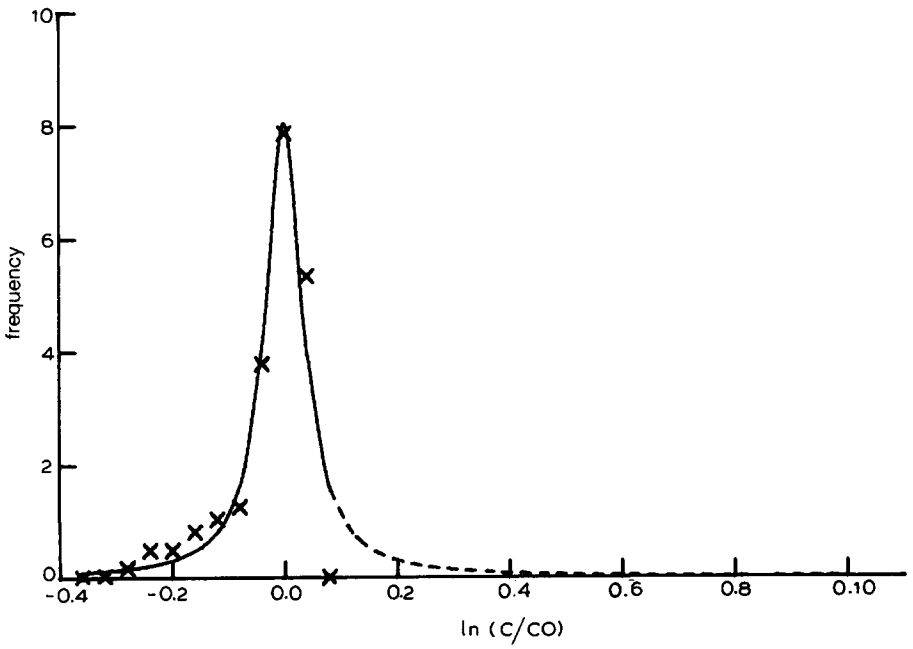

Fig. 14. Cole and Cole distribution function fitted to the capacity distribution profile of a Li (100) plane on a logarithmic scale.

(VI) CONCLUSIONS

It is possible to define a metal layer capacity C_m originating from charge redistributions at the electrode surface as a function of potential. The capacity is distributed over the electrode surface, as a consequence of the crystalline structure. This distribution causes the interfacial impedance not to behave in a purely capacitive way but to be complex.

The values of the calculated capacities lie below the experimental range and indicate that the metal layer capacitance in an electrolyte solution differs from its value in vacuum. With linear clusters of moderate size (4–8 atoms) one can obtain a reliable estimate of the average capacity values of large 3-dimensional clusters (20–24 atoms).

ACKNOWLEDGEMENTS

The authors wish to thank Dr. F.B. van Duijneveldt for helpful discussions and Dr. A. Hamelin and Drs. G. Brug for their active interest in this work. The gold electrodes were prepared at the Laboratoire d'Electrochemie Interfaciale du CNRS, Meudon, France, in accordance with the instructions of Dr. A. Hamelin.

REFERENCES

1 H.L.F. von Helmholtz, Ann. Physik, 2 (1853) 89.
2 G. Gouy, C.R. Acad. Sci., 149C (1910) 654.
3 D.L. Chapman, Phil. Mag., 25 (1913) 475.
4 O. Stern, Z. Elektrochem., 30 (1924) 508.
5 See e.g. P. Delahay, Double Layer and Electrode Kinetics, Interscience, New York, 1965.
6 R.J. Watts-Tobin, Phil. Mag., 6 (1961) 133; R. Parsons, J. Electroanal. Chem., 59 (1975) 229; W.R. Fawcett, S. Levine, R.M. de Nobriga and A.C. Mc Donald, J. Electroanal. Chem., 111 (1980) 163.
7 O.K. Rice, Phys. Rev., 31 (1928) 1051.
8 W. Schmickler, J. Electroanal. Chem., 150 (1983) 19.
9 A.A. Kornyshev, W. Schmickler and M.A. Vorotyntsev, Phys. Rev. B, 25 (1982) 5244.
10 J.P. Badiali, M.L. Rosinberg and J. Goodisman, J. Electroanal. Chem., 143 (1983) 73.
11 J.P. Badiali, M.L. Rosinberg and J. Goodisman, J. Electroanal. Chem., 150 (1983) 25.
12 R. Smoluchowski, Phys. Rev., 60 (1941) 661.
13 G. Brug, M. Sluyters-Rehbach, J.H. Sluyters and A. Hamelin, J. Electroanal. Chem., submitted.
14 M. Sluyters-Rehbach and J.H. Sluyters in A.J. Bard (Ed.), Electroanalytical Chemistry, Vol. 4, Marcel Dekker, New York, 1970, pp. 1–128.
15 R.D. Armstrong and W.I. Archer, J. Electroanal. Chem., 87 (1978) 221.
16 K.S. Cole and R.H. Cole, J. Chem. Phys., 9 (1941) 341.
17 C.J.F. Böttcher and P. Bordewijk, Theory of Electric Polarization, Vol. 2, Elsevier, Amsterdam, 1978, Ch. 9.
18 N.D. Lang and W. Kohn, Phys. Rev. B, 1 (1970) 4555.
19 Ch. Kittel, Introduction to Solid State Physics, Wiley, New York, 1968, p. 12.
20 C.C.J. Roothaan, Rev. Mod. Phys., 23 (1951) 69.
21 F.B. van Duijneveldt, IBM Technical Report RJ945, IBM Thomas J. Watson Research Center, Yorktown Heights.
22 F.B. van Duijneveldt, private communication, 1983.
23 H.D. Cohen and C.C.J. Roothaan, J. Chem. Phys., 43 (1965) S34.
24 IBMOLH Program System, Internal Report, Theoretical Chemistry Group, Utrecht, 1976.
25 J. Demuynck, M-M. Rohmer, A. Strich and A. Veillard, J. Chem. Phys., 75 (1981) 3443.
26 R.W.G. Wychoff, Crystal Structures, Vol. 1, Wiley, New York, 1963.
27 F.L. Pilar, Elementary Quantum Chemistry, McGraw-Hill, New York, 1968, Ch. 18.